

# Non-dispersive infra-red (NDIR) measurement of carbon dioxide at 4.2 $\mu$ m in a compact and optically efficient sensor.

Jane Hodgkinson<sup>a\*</sup>, Richard Smith<sup>b</sup>, Wah On Ho<sup>b</sup>, John R Saffell<sup>b</sup> and Ralph P Tatam<sup>a</sup>

a Department of Engineering Photonics, School of Engineering, Cranfield University, Bedfordshire, MK43 0AL, UK

b Alphasense Ltd, 300 Avenue West, Skyline 120, Great Notley, Essex CM77 7AA, UK

\* corresponding author: email [j.hodgkinson@cranfield.ac.uk](mailto:j.hodgkinson@cranfield.ac.uk)

tel +44 (0)1234 750111 ext 5364

## ABSTRACT

Non-dispersive infra-red (NDIR) gas detection has enjoyed widespread uptake as a result of development of devices in the standard miniature format for gas sensors, consisting of a cylinder with external dimensions of 20 mm diameter x 16.5 mm height. We present a new design for such a sensor, making use of low-cost injection moulding technology. The design pays particular attention to the problem of maintaining a high optical throughput while providing an acceptable optical pathlength for gas detection. A detailed analysis of the design is presented, with the results of optical raytracing, showing a raytrace estimate for 4% of the total emitted radiation reaching each of two separated detector elements and a pathlength of 32 mm. Finally, we show experimental results obtained with as-manufactured devices, with a short-term limit of detection for carbon dioxide (CO<sub>2</sub>) estimated at 1 ppm or a noise equivalent absorption (NEA) of 3 x 10<sup>-5</sup> AU.

## Highlights

- New design of non-dispersive infra-red (NDIR) sensor for CO<sub>2</sub> and other gases
- Standard miniature format for gas sensors – a cylinder 20mm D x 16.5mm H
- Raytrace - estimated 32mm pathlength
- Manufactured in volume using gold-coated injection-moulded reflective optics
- Short-term limit of detection 1ppm CO<sub>2</sub>, noise equivalent absorbance 3x10<sup>-5</sup> AU

## Keywords

Non-dispersive infra-red, NDIR, gas detection, optical absorption, carbon dioxide

## 1 INTRODUCTION

Non-dispersive infrared (NDIR) gas sensing is one of the most widely used optical gas detection techniques, and there is a wide range of cell designs in commercial manufacture [1]. For some gases, notably carbon dioxide (CO<sub>2</sub>), alternative (non-optical) technologies are unsuitable and therefore CO<sub>2</sub> detection in low-cost, volume applications often incorporates an NDIR sensor. These applications include heating, ventilation and air conditioning (HVAC) control [2], industrial safety especially in the brewing industry (CO<sub>2</sub> is an asphyxiant), process control and capnography (the measurement of time-resolved CO<sub>2</sub> concentration in exhaled breath) for patient monitoring for example during anaesthesia [1].

There are few alternative sensor technologies capable of detecting CO<sub>2</sub> at ppm concentrations. Devices have been developed based on the electrochemical principle [1] and research is also underway on metal oxide semiconductors for CO<sub>2</sub>. However, both techniques are known to cross-respond to other gas species, including water vapour, whereas NDIR sensors for CO<sub>2</sub> are considered to be specific to that species alone [1]. Furthermore the development of metal oxide sensors capable of detecting CO<sub>2</sub> below 2,000ppm is “the biggest challenge” according to a recent review [3].

Over the last decade, the commercial market has become populated with small footprint gas sensors based on the NDIR principle [4]. The dimensions of these sensors (a cylinder 20 mm diameter x 16.5 mm high) follow a default standard for the gas sensor industry that we will refer to throughout this paper as the standard miniature format. Thus, equipment manufacturers need not alter the dimensions of their housings when switching to NDIR sensors.

These sensors are low cost, having few components (typically a simple microbulb light source, gold coated reflective light path and detector) [5]. The microbulbs used in conventional NDIR sensors have two main advantages; their spectral emission is relatively high (2 mW per steradian in a FWHM bandwidth of 0.17 μm at 4.2 μm, for one example [6]) and the cost is low (\$1-2 [6]). A key to the miniaturisation of this technology has been the integration of multiple detectors and filters into a small single package, typically a 9mm diameter TO-5 can [7]. Commercially available sensor designs in the standard miniature format include a dual ellipsoid / reflector / ellipsoid arrangement [8], a pathlength arranged in the form of a spiral around the bulb / detector [9], and a mini integrating sphere with a rough internal surface, in which the light bounces around the internal cavity at random until it is absorbed by the sidewalls, the gas sample, or the detector [4]. However, detailed optical analysis of these compact designs has been limited, as is the use of injection moulding technology, which offers a potentially wider range of design options. A recent design with an LED source and photodiode integrated on an electronic chassis uses injection moulded reflective optics [10], with the simplest optical design having both emitter and detector as close as possible to the centre of a hemisphere. However its use of an LED is restrictive as such devices are currently significantly more costly than microbulbs.

Research in this area has concentrated on the following requirements; (i) the need for compact cells, (ii) maximising the pathlength to optimise sensitivity, and (iii) the need to maximise the proportion of light coupled through the cell to the detector, in order to overcome the detector noise limit.

Fonollosa *et al* have developed a high numerical aperture (NA) Fresnel lens formed in silicon (transmissive in the mid IR) to make a light-efficient and ultra-compact dual band detector [11]. The detector module has been integrated into a system for measuring ethylene in agricultural storage, with a 30ppm detection limit [12]. Further miniaturisation may also result from work to integrate detectors and filters on a single base substrate [13].

The light collection efficiency of an optical system may be defined using the 3D étendue, equal to the product of the light beam's area and its solid angle. The proportion of light passed from one element of the system to the next is proportional to the étendue, and the overall throughput (T) can be defined as [14]:

$$T = A\Omega\rho \quad (1)$$

At the limiting aperture,  $A$  is the area of the aperture,  $\Omega$  is the solid angle and  $\rho$  accounts for additional losses in the system, for example due to the reflectivity of mirrors being less than 100%. To design a high efficiency cell, one must maintain a high étendue throughout the system, which demands the use of large apertures and / or high NA optics throughout. Constraints on the cell volume will therefore impact on the optical pathlength, or optical efficiency, or both. It is for this reason that the design of a compact, optically efficient cell presents a challenge. Typically within a 20 mm diameter x 16.5 mm high sensor (external dimensions) are the 9mm diameter detector and 3.2 mm diameter x 6.4 mm long cylindrical microbulb, which leaves little room for manoeuvre when designing the optical path.

Various groups have reported studies of novel gas cell designs using a ray tracing approach. Mayrwöger *et al* have used the Zemax software package to evaluate 3 different cell designs including a hollow, internally reflective tube (25mm long x 3mm diameter), an internally reflective ellipsoid (principal axes 55 mm and 20 mm) and a spiral design within a cylinder of dimensions 30 mm diameter x 10 mm height [15]. Each design incorporated a standard microbulb and a single element detector within a 9 mm diameter TO-5 can. For the latter two designs, mean optical pathlengths of 140 mm and 980 mm were reported from the ray trace simulations. The first (tube) design was used in combination with a bolometer detector to measure CO<sub>2</sub> with a limit of detection of around 150ppm [16].

Sieber *et al* have also reported a method for optimising a ray traced design for a chamber containing a curved surface that focused light from source to detector [17]. In particular, they showed the effect of positioning of the source on the irradiance distribution in the chamber, and reported how the overall gas detection performance was to be modelled. Their chamber was 42 mm long, with a mean pathlength of 60 mm. An optical cell with similar dimensions and elliptical reflectors has also been developed, and used by Hók *et al* in

the detection of breath ethanol [18]. Multiple reflections provided a pathlength of 210 mm within a package of approximately 40 mm x 40 mm x 14 mm.

Viola has reported on the development of a multipass NDIR cell with an acceptance NA of 0.22 and source / detector areas of 5x5 mm each [14]. Collection efficiency was 3.7 sr mm<sup>2</sup> and overall throughput (taking into account multiple reflections from gold surfaces with 95% reflectivity) was estimated to be 2.2 sr mm<sup>2</sup>. The overall physical length of the gas cell was >120 mm, and multiple passes between two off-axis parabolic mirrors and two retroreflectors yielded an optical pathlength of 940 mm. Optical performance has been validated and the device has been used to detect ammonia at 10.5 μm [19].

Despite this activity, to date none of this reported work has been applied to sensors as small as the standard miniature format. In this paper, we report on the modelling and realisation of a novel gas cell design that fits within these external dimensions of a 20 mm diameter x 16.5 mm height cylinder, translating to internal dimensions for the optics of 17.5 mm diameter and 10.5 mm height.

## 2 PRINCIPLE OF OPERATION

For monochromatic light, the Beer-Lambert law gives the level of light  $I$  transmitted through an absorbing medium such as a gas [20],

$$I = I_0 \exp(-\alpha \ell) \quad (2)$$

Where  $I$  is the light transmitted through the gas cell,  $I_0$  is the light incident on the gas cell,  $\alpha$  is the absorption coefficient of the sample (units of cm<sup>-1</sup>) and  $\ell$  is the cell's optical pathlength (units of cm). The absorption coefficient  $\alpha$  is the product of the gas concentration (for example the partial pressure in atm) and the specific absorptivity of the gas  $\epsilon$  (for example in cm<sup>-1</sup>atm<sup>-1</sup>). At low values of  $\alpha \ell$ , this approximates to a linear relationship as follows:

$$I \approx I_0(1 - \alpha \ell) \quad (3)$$

Figure 1 shows a schematic diagram of a simple NDIR gas sensor. Typically, emission from a broadband source (such as a microbulb [21]) is passed through two filters, one covering the whole absorption band of the target gas (in the active channel), and the other covering a neighbouring non-absorbed region (the reference channel). Typical filter characteristics for CO<sub>2</sub> measurement are shown in Figure 2, alongside the gas absorption spectrum. Provided that the chosen active and reference channel filters do not overlap significantly with the absorption bands of other gas species present in the application, cross-sensitivity to other gases lies below the limit of detection. Fortunately for CO<sub>2</sub> sensing the filters shown in Figure 2 are spectrally located far from absorption bands of potential interferents such as water vapour or hydrocarbons at typically

encountered concentrations. The spectroscopic effect of dust scattering is a potential problem at low limits of detection [1], but dust filters are commonly used anyway to protect the optics so for closed or diffusion cells the problem is avoided.

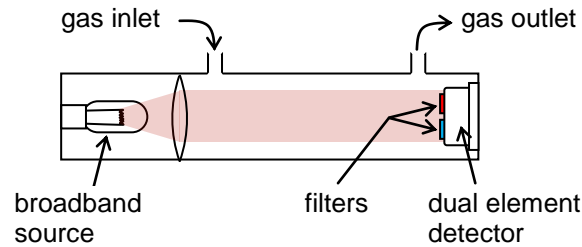


Figure 1. Schematic diagram of a linear non-dispersive gas sensor with optical pathlength in the range 3-20cm. The source and detector are usually placed inside the cell to avoid baseline drifts that would otherwise be caused by variations in the background CO<sub>2</sub> concentration in the external optical path.

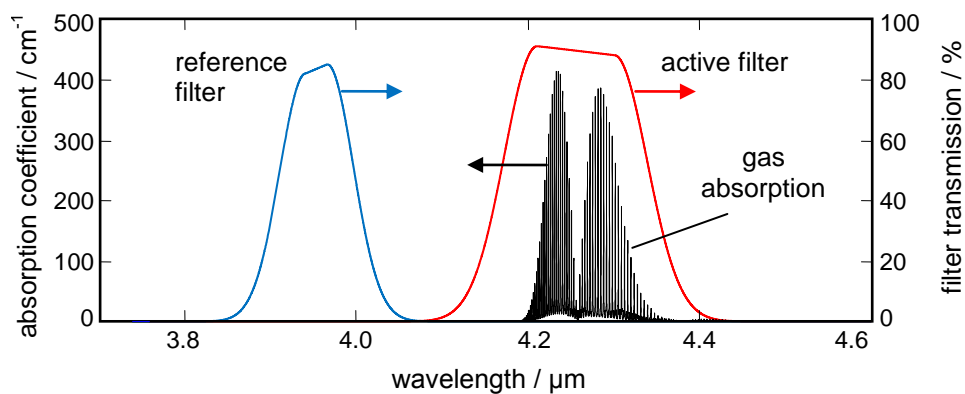


Figure 2. Illustration of NDIR measurement principle. The absorption spectrum of CO<sub>2</sub> (calculated from the HITRAN database [22]) is superimposed on the transmission spectra of active and reference channel filters (approximated from ref [7]).

NDIR gas sensing relies on the strength of optical absorption in the mid IR, which can be of the order of 100 times greater than that in the near IR [5]. Thus, even with short pathlengths (3-10 cm), using relatively unsophisticated sources (microbulbs) and uncooled detectors (pyroelectric or thermopile), respectable limits of detection may be achieved (eg 2-10 ppm for CO<sub>2</sub> [2]), and detection limits as low as 0.1 ppm can be obtained using more sophisticated equipment [23].

Transmission through the active channel comprises the integrated gas absorption:

$$I = I_0 \int E_S(\lambda) T_A(\lambda) \exp[-\alpha(\lambda)\ell] d\lambda \quad (4)$$

Where  $E_S$  is the emission envelope of the source and  $T_A$  is the transmission of the active channel filter. For low  $\alpha\ell$ , equation (4) is again linear with  $\alpha$ , and therefore with gas concentration.

In the region of linear operation, we can adapt equation (3) to give the absorbance;

$$\alpha'\ell = 1 - \frac{I_A}{I_{0A}} \quad (5)$$

Where the subscript  $A$  denotes the active channel, and  $\alpha'$  is a pseudo absorption coefficient that follows from equation (4). The performance of NDIR systems can be estimated in terms of the minimum detectable change in optical power,  $\Delta I/I_0$ . For NDIR the figure corresponds to a noise equivalent absorbance (NEA) where the “absorbance” concerned is an integrated effective absorbance over the measurement band. Aleksandrov *et al* have claimed an NEA better than  $10^{-3}$  AU (100 ms response time) [24]. In this case, a minimum detectable  $\text{CO}_2$  concentration of 25 ppm was estimated, using a 4 cm pathlength.

A reference channel is used to compensate for changes in the emission of the source, which are assumed to affect the reference and active channel wavelengths in equal proportion. In the case of incandescent sources, these changes tend to result from either (i) temperature fluctuations of the filament, or (ii) gradual blackening of the inside of the glass envelope and loss of radiating area caused by filament evaporation; in either case the assumption is valid to first order. Thus, we measure the reference channel intensity  $I_R$  as a substitute for  $I_0$  and define the normalised absorbance signal  $S$  as;

$$S = 1 - \frac{I_{0R} I_A}{I_{0A} I_R} \quad (6)$$

where the subscript  $R$  denotes the reference channel.  $S$  is unitless but typically described in “absorbance units” (AU). The value of  $I_{0R}/I_{0A}$  may be determined by flushing the sample cell with clean,  $\text{CO}_2$  free air. It is this quantity,  $S$ , corrected for drift using the reference channel, that we report in our results below.

Because broadband light sources are often highly divergent, detection limits over long pathlengths are dependent on the source power emitted within a defined spectral window, and the detector noise. For the latter, a normalised figure of merit may be used, the specific detectivity or  $D^*$  [20], equal to the signal to noise ratio (SNR) when used in uniform irradiance, normalised for detector area  $A_d$  and measurement bandwidth  $\Delta f$ .

$$D^* = \frac{\sqrt{A_d \Delta f}}{\text{NEP}} \quad (7)$$

Where NEP is the noise equivalent power. The units of  $D^*$  are typically expressed as  $\text{cm}\cdot\text{Hz}^{1/2}\cdot\text{W}^{-1}$ .

### 3 DESIGN PRINCIPLES

Our sensor was designed to detect CO<sub>2</sub> gas via its well-known absorption band centred at 4.2µm, as shown in Figure 2, using standard source and detector components. A dual element detector was chosen with active and reference channels defined by bandpass filters centred at 4.26µm and 3.95µm; typical manufacturer's transmission spectra are shown in Figure 2 (Perkin Elmer G2 and G20 filters). A broadband emitter was also chosen (Gilway 1600) consisting of a coiled-coil incandescent filament within a glass bulb. The tungsten filament is assumed to have grey body (emissivity < 1) emission with a filament temperature of around 3000K. The glass bulb is known to have approximately 40% transmission at 4.2 µm, falling to zero transmission above 5 µm [25]. As both emitter and detector are in standard use, our work concentrated on the design of the optical path in the cell.

We have assumed that our source was the bulb filament rather than the bulb envelope. As the glass bulb is known to absorb a proportion of the light emitted by the filament, it is possible that it could warm and cool at the source modulation frequency. If so it would then re-emit light as a grey body, forming a larger effective source. We checked our assumption by measuring the external temperature of the glass bulb using a thermocouple soldered to the glass, in good thermal contact, while driving the source with a 0-5V square wave at a low frequency of 1.5 Hz. We observed no measurable synchronous change in the mean temperature of 40.8 °C and a small non-synchronous variation of ± 0.1 °C RMS. This rules out significant synchronous emission by the bulb envelope.

We used the Zemax [26] commercial raytracing package for the design process. In common with Mayrwöger *et al* [15], we required use of non-sequential raytracing in three dimensions, in which rays are permitted to strike any object, in any order. This feature increased processing time, such that it became impossible to use a number of automated optimisation and tolerancing features, however it was essential for our analysis. Non-sequential raytracing takes automatic account of multiply reflected beams and of beams that for example leave the source and are then reflected back towards it, which as we will see later indeed occurs in our design. We also made use of the ability of this package to export to, and import from, commercial CAD software used in manufacturing design.

To design an optically efficient NDIR cell, we aimed to maintain a high étendue along all stages of the optical path. Ideally, the limiting aperture would be provided by the detector, whose design was fixed. We designed for a standard two element pyroelectric detector from Perkin Elmer (PYS3228) however the design also needed to accommodate potential use of alternative detectors, both pyroelectric (eg Infratec LIM 122, HL Planar TS 105, Pyreos PY-ITV-DUAL) and thermopile (eg Perkin Elmer TPS 2534, Infratec LIM 212, Dexter DR34). Our standard detector had two photodetector elements of size 1.5mm x 1.5mm, centres separated by 3.4 mm, and an acceptance half-angle of 38.5°, giving an individual 3D étendue of 3.5 sr mm<sup>2</sup> for each one. However, we needed to create an even level of illumination over both detectors, therefore if we define the acceptance aperture as the 1.5 mm x 4.9 mm rectangular area covering both photodetector elements, the étendue is

increased to  $11.4 \text{ sr mm}^2$ . The consequence is that unless the light path is split, there is a minimum of 40% loss of light between the two detector elements.

We aimed to collect as much light from the source as possible, within the space constraints of the sensor. The source consisted of an extended filament lamp (filament 1.3mm long, 0.2mm radius, coiled coil with 6 main coils) emitting in all directions. Simplifying this to a cylinder with isotropic emission gives a maximum 3D étendue of  $6.5 \text{ sr mm}^2$ , therefore in principle it might be theoretically possible to transfer all the emission from this emitter to the rectangular area covering both detector elements giving an ideal value of  $2.0 \text{ sr mm}^2$  per detector element.

We chose to use a compound parabolic collector (CPC), also known as an off-axis paraboloid, to collect the forward-emitted light. These non-imaging devices have the property of maintaining an étendue along their length and partially collimating emission from a source by increasing the emitting aperture [27]. Ideally we would use a longer CPC with exit aperture limited to  $\pm 10^\circ$ , however two factors prevented this, (i) a requirement for additional space around the source to allow for dimensional tolerancing and thermal management (the source outer glass envelope being hot), and (ii) space constraints that limited the length of the CPC.

Manufacturing tolerances on the position of the source filament within the outer envelope limit the side-to-side filament position to  $\pm 0.5\text{mm}$ , and furthermore there is potential for the filament to move or bow out as a result of thermal expansion, or to move if the sensor is prone to shock or vibration. To reduce the effects of these movements, we placed a hemispherical reflector behind the filament to collect the backward-emitted light and return it to an equivalent point on the filament but on the opposite side. It is recommended to use such devices with off-axis filaments in illumination systems [27], however space constraints prevented use of an off-axis design.

One of the most important design considerations, by reference to equation (6), is that the relative proportions of light falling on the two elements of the detector (in the absence of gas) should remain constant between zeroing and use. To this end, the optical path was designed to be symmetric about a mirror plane passing between the two detector elements, such that they would be mirror images of each other in this plane. The hemispherical reflector behind the source increased the level of symmetry for light emitted from one or the other side of the filament. The sensor symmetry also needed to be maintained in the face of manufacturing tolerances.

A final design consideration was manufacturability. The sensor device was built from injection moulded thermoplastic with a gold reflective coating, making it a low cost device for volume applications. For this reason, the optical path had to consist of a limited number of injection mouldable parts, ie parts with no re-entrant spaces, ideally requiring very simple alignment.



## 4 OPTICAL DESIGN

We have previously reported the essentials of our optical design and its initial results [28]. The optical design is shown in Figure 3 as a line drawing and screenshot from the Zemax [26] raytracing software. It was realised as two injection mouldable halves, joined together during manufacture in the manner of a clam shell. The source and detector were placed back-to-back and the optical path folded around the cylinder from one to the other. Embedded Zemax objects were used to model all the optical elements including the bulb filament, CPC and mirrors. To model this design repeatably (ie with minimal differences between raytracing runs with different random number generator seeds) using non-sequential raytracing required  $10^6$  rays from the source; for simplicity only 100 “construction rays” are shown in Figure 3. A conservative estimate of 95% was used for the gold surface reflectivity, however for simplicity we assumed that there was no scattering present in the cell. We also made no attempt to quantify the effect of the join line between the two halves of the clamshell, which was expected to have a strong scattering effect.

The design was exported from Zemax using embedded Zemax objects, which were then converted into a 3D mechanical space-filling design with various construction elements including a header onto which the bulb and detector are mounted. This design was re-imported to Zemax and re-modelled to confirm that the mechanical design process had not impacted on the optical design, and also that CAD surface tolerances were adequate. The result was a minor (2%) reduction in the proportion of light falling on the detector.

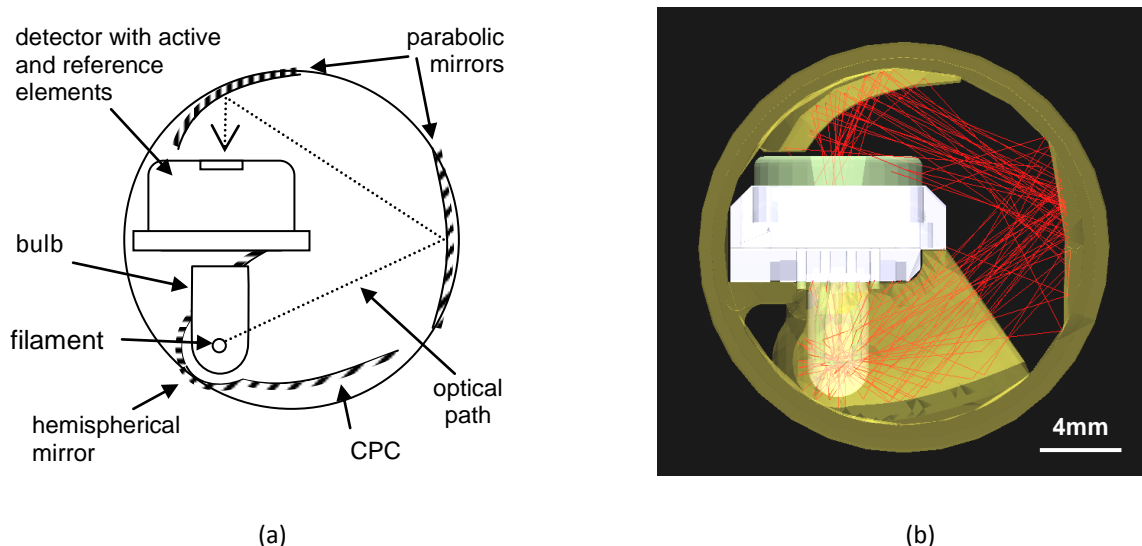


Figure 3. Sensor design, top view. (a) Schematic line drawing, (b) Zemax screenshot of the CAD assembly shown with 100 construction rays and dual element pyroelectric detector. The bulb filament points vertically into the page, and the active and reference detector elements are located along a line also normal to the page.

## 4.1 Light efficiency

The total proportion of light falling onto each detector element was estimated by raytracing. We did not consider losses within the detector or reflections from the detector filters as these are accounted for in manufacturers' data, which specifies filter transmission as well as detector responsivity according to the light intensity at the external aperture. A number of design compromises had to be made, listed below, that reduced the light efficiency from what was otherwise achievable.

- (i) The position of the filament was altered empirically (moving it forward slightly) to give better tolerance to sideways or forward-and-back motion of the filament. This had the effect of reducing the collection efficiency as the filament was no longer exactly at the entrance to the CPC.
- (ii) The microbulb was inserted into the CPC through a hole, resulting in an area that could no longer reflect light into the optical path. The position of the hole was altered to facilitate manufacture, which reduced the transmission efficiency of the CPC.
- (iii) The bulb and detector were located on a header which also provided their electrical contacts. The physical size of the header presented a substantial shadow in the optical path, visible in Figure 3 where the header protrudes through the CPC.
- (iv) As mentioned above, for a perfectly even distribution of light across the detector there is a minimum 40% loss of light due to that falling between the two elements.
- (v) Use of a gold coating with an estimated 95% reflectivity led to a 15% proportional reduction in the total collected light in the raytraced model, from 4.7% to 4.0% falling onto each detector element.

These losses reduced the throughput to  $6.5 \text{ sr mm}^2 \times 4\% = 0.26 \text{ sr mm}^2$  per detector element or  $0.52 \text{ sr mm}^2$ , in total. The final acceptance angles estimated for the standard detector from the raytrace model were approx  $\pm 25^\circ$  (top view) and  $\pm 17^\circ$  (side view). That we were unable to achieve light collection over the full potential field of view of the detector is attributed to the overall space constraints of the device. However, there is some advantage to having a restricted range of angles: we prefer to have as much light as possible concentrated within a narrow cone around normal incidence. The interference filters used in the detector package are designed for normal incidence; off-axis rays would otherwise contribute to a shift in the centre wavelength of the passband and their angular distribution would give rise to a broadening of the passband.

Further effects are expected to reduce the optical efficiency of real devices. Firstly, real gold surfaces are likely to exhibit some scattering caused by moulding imperfections, residual machining lines on the mould tool or stray dust. It is to be expected that such scattering would predominantly remove light from the intended optical path. Secondly, our design requires a weld line between the two injection moulded clam shell halves. We did not model this but again we would expect the predominant effect to be to scatter an unquantified proportion of light out of the intended optical path, reducing device throughput.

## 4.2 Pathlength estimation

The optical path was deduced from information about traced rays, saved by Zemax to a text file, including the location, length and relative intensity of each ray's segment, plus codes to identify the objects from which the ray was reflected or transmitted. The number of rays that can be saved by Zemax is limited to 10,000. It was possible to target only rays that had fallen on one or the other detector elements, giving a total sample of 20,000 rays.

The text file thus obtained was analysed using a Mathcad [29] program written specifically for the purpose. The program identified ray segments that could encounter gas, and summed their lengths along the ray. For example, a ray passing from the filament through the bulb cavity would not encounter any gas in the cell until it left the bulb glass envelope. Many rays subsequently passed back through the bulb cavity and / or the glass envelope.

Once the total effective length and relative intensity of each ray had been calculated, a probability distribution function was constructed, shown in Figure 4. The mean effective pathlength was calculated to be 32 mm. Figure 4 shows two pairs of peaks in pathlength distribution whose centres are separated by approximately 1.7 mm, with the longer pathlength peak being slightly broader. This is attributed to the use of the hemispherical reflector behind the source, which was located 0.5 mm from the bulb envelope at its closest point, typically adding an additional 1.4-1.5mm pathlength. The second, much smaller pair of peaks is believed to show more highly skewed rays, in both cases typically striking the hemispherical reflector.

The 30.4mm peak comprises mainly of rays reflected 3 times, from the CPC, right hand mirror and upper mirror (in Figure 3 (a)), with a small minority of rays that were directed forwards and did not strike the CPC so only encountered 2 reflections. The second peak at 32.3mm consists mainly of rays that struck the hemispherical mirror first and then exhibited similar behaviour, with 4 reflections in total. The remaining peaks at 35.0mm and 36.4mm also consist mainly of rays having 4 reflections in total.

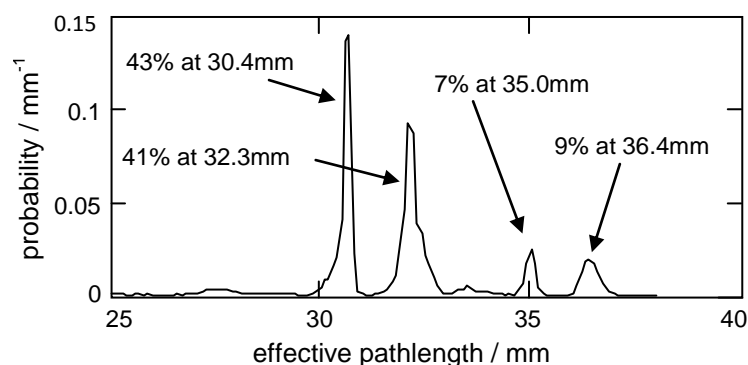


Figure 4. Probability distribution function of effective pathlengths for the NDIR sensor, as modelled by Zemax [26].

A pathlength of the order of 30mm is not untypical of devices of this size [8,9]. For measurement of trace concentration of carbon dioxide, clearly it is desirable to have as long a pathlength as possible. However, many CO<sub>2</sub> sensors are required to operate over a wide dynamic range, in order to measure concentrations of up to 100% for example in process control applications. The nonlinearity inherent in such devices, stemming from equation (2), limits the resolution at high concentrations when combined with detector noise. Longer pathlength devices can reach saturation levels if used at higher concentrations. A high degree of nonlinearity is evident in experimental results for our device, shown in Figure 8 below.

### 4.3 Sensor construction

The optical design described above was exported from Zemax as a computer aided design (CAD) model, which was used to machine an injection mould tool designed for volume manufacture. From this, injection moulded thermoplastic parts were created as two halves of the clam shell type design and coated with gold for mid IR reflection. Figure 5 shows an exploded diagram of the sensor construction. The two halves defining the optical path were joined together during manufacture so as to enclose the source and detector. At the top of the cylinder (out of the optical path) were located a number of holes and a dust filter, allowing the gas sample to diffuse into the entire sensor body. At the bottom was the printed circuit board (PCB), with connection pins.

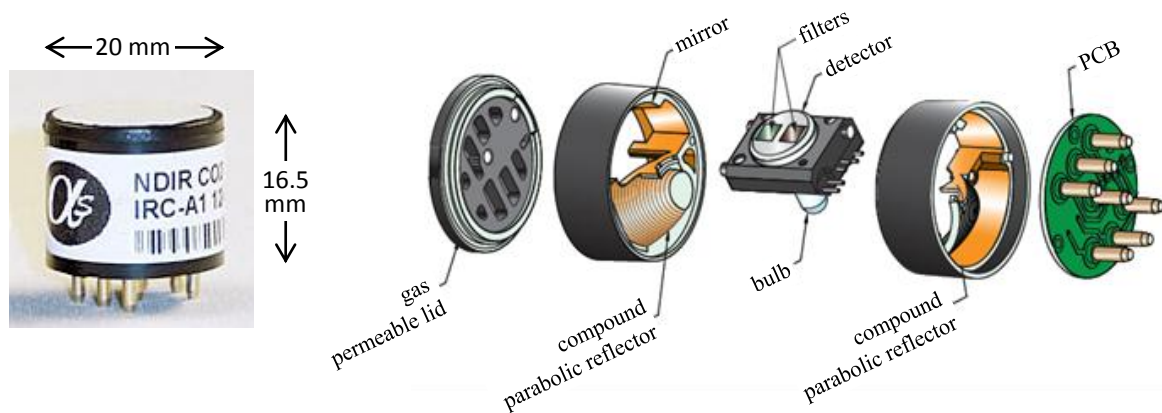


Figure 5. Photograph and exploded diagram of manufactured NDIR sensor device, showing the two symmetrical, gold coated optical parts that defined the optical path.

Because we made our first devices with a production standard injection mould tool, our initial optical testing was representative of final, as-manufactured sensors. The experimental tests presented here were made using standard components, namely a microbulb (Gilway 1600) and uncooled dual element pyroelectric detector (Perkin Elmer PYS3228).

## 5 EXPERIMENTAL RESULTS

### 5.1 Optical and electronic characterisation

To measure the amount of light collected at the detector, the microbulb was first modulated at a frequency of 1 Hz with a square wave of 0-5 V. The 1 Hz modulation frequency was chosen because the detectors were characterised at this frequency by the manufacturer. The detector, which incorporates an internal FET based amplifier, was driven with a 5V supply. The RMS detector voltage was recovered using a lock-in amplifier (Stanford SR850) on the reference and active channels separately.

The responsivity of the detector is quoted by the manufacturer to be  $3.5 \times 10^3$  V/W (typical figure) for the unfiltered detector elements at a frequency of 1Hz, defined by the level of light incident at the filter location. This yields an RMS modulated intensity at the detector element of  $13\mu\text{W}$  (reference channel), transmitted through the reference bandpass filter with a typical FWHM bandwidth of  $0.10 \mu\text{m}$  and peak transmission of 80%.

Detector noise was measured using an FFT spectrum analyser (Stanford SR780) and found to be approximately flat in the region from 0.2 – 12.5Hz. Both channels exhibited detector noise in this frequency region of approximately  $1.25 \mu\text{V Hz}^{-1/2}$ . Following equation (6), this would lead to a combined detector noise of  $1.8 \mu\text{V Hz}^{-1/2}$  if the zero readings were established with negligible noise (over a longer time period), or  $2.5 \mu\text{V Hz}^{-1/2}$  if they were established with similar levels of noise as the actual measurements. Modulating our light source at 2 Hz (as in device tests below), we recorded RMS signals of 20 mV, therefore if overall sensor noise were detector noise limited we would see a best case NEA of  $1.3 \times 10^{-4} \text{ Hz}^{-1/2}$ .

### 5.2 Gas response and limit of detection

The sensor was tested using the experimental configuration shown in Figure 6. For these tests we used a modulation frequency of 2Hz, which is recommended for the device in use, driving the microbulb with a 0-5V peak-peak square wave via a signal generator (Stanford DS345). Figure 7 shows a typical recorded trace. A laboratory power supply (Weir 413D) provided a 0-5V supply for the detector pre-amplifiers, and signals were recovered from each channel with a lock-in amplifier (Stanford SR850). The lock-ins were matched, with identical settings (time constant 10s, 24dB/octave roll-off) which gave each an equivalent noise bandwidth (ENBW) of 7.8mHz. The lock-in time constant of  $\tau = 10\text{s}$  corresponds to a response time to reach 90% of the final value ( $t_{90}$ ) of 23s, assuming a temporal response taking the form  $1 - \exp(-t/\tau)$ .

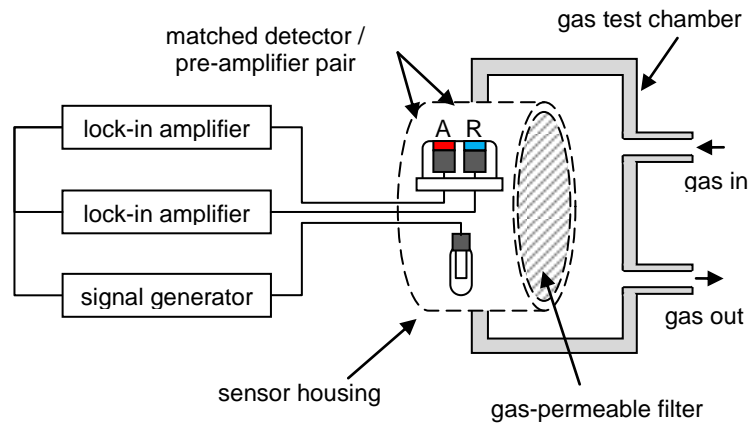


Figure 6. Schematic configuration for sensor testing using lock-in amplifiers (not to scale). See Figure 3 for the optical configuration of the sensor cell. A and R refer to the active and reference channels respectively.

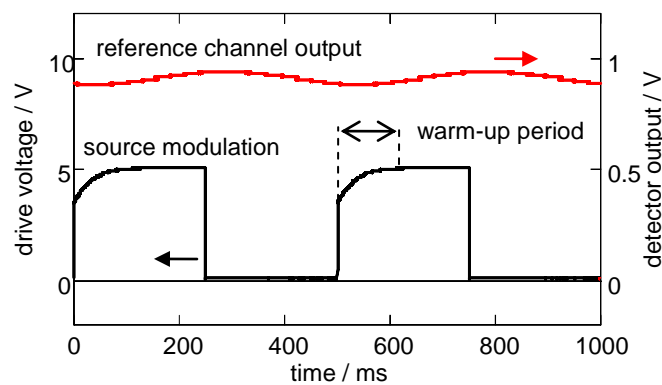


Figure 7. Signal trace and source modulation directly recorded using a digital oscilloscope. Upper trace: detector output (reference channel only shown for clarity), lower trace: source drive voltage.

Test gases were supplied from certified cylinders (Scott Specialty Gases) with CO<sub>2</sub> concentrations of 0 ppm (+1/-0, HC and CO<sub>2</sub> free air), 2006 ppm ( $\pm 1$  ppm) CO<sub>2</sub> in air and 19.9% (199,000 ppm) CO<sub>2</sub> in air. Here, “air” refers to a synthetic mixture of nitrogen and oxygen, without any CO<sub>2</sub> background (ambient air contains a background of around 380 ppm CO<sub>2</sub>). Gas from the cylinders was fed into a bank of mass flow controllers (Teledyne Hastings HFC-302 with THPS-400 controller) with ranges of (i) 0-1000 cm<sup>3</sup>/min, (ii) 0-1000 cm<sup>3</sup>/min, (iii) 0-100 cm<sup>3</sup>/min and (iv) 0-10 cm<sup>3</sup>/min. This system was used to control flow rates from the two cylinders, with downstream mixing generating a series of mixtures of different concentrations in the range 0-2006 ppm CO<sub>2</sub> in air or 0-19.9% CO<sub>2</sub> in air. For each step change in concentration applied, a total of 3 minutes was allowed for passage of gas down the connecting pipework, diffusion into the cell and settling of the lock-in

amplifiers before taking readings. At each concentration step, signals from the active and reference channels were recorded simultaneously and the normalised signal  $S$  calculated according to equation (6). The values of  $I_{OR}$  and  $I_{OA}$  used to normalise the measurement were established in the same way by supplying zero air (free from  $\text{CO}_2$ ) to the test chamber prior to each gas measurement and again taking readings simultaneously on both channels.

The results are shown in Figure 8 and demonstrate a characteristic nonlinearity stemming from equation (2) at high concentrations. At low concentrations (below approximately 500 ppm) the response is linear and can be used to estimate the limit of detection. The short-term noise equivalent absorbance (NEA) for the sensor was estimated to be  $3 \times 10^{-5}$  AU from a zero stability analysis (see below, Figure 9), equivalent to  $3 \times 10^{-4} \text{ Hz}^{-1/2}$ . A short extrapolation of our data in the linear region leads to an estimate for the limit of detection of approximately 1 ppm.

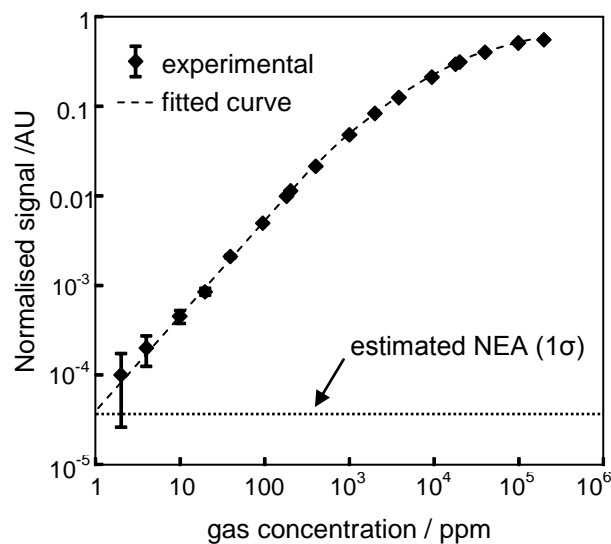


Figure 8. Normalised signal ( $S$  according to equation (6)) as a function of gas concentration in the range 0-200,000 ppm (0-20%vol). The estimated noise suggests a limit of detection of approximately 1 ppm.

This estimate of measurement uncertainty is approximately 3 times worse than would be the case if the sensor were purely limited by detector noise, and implies that there were other factors involved. Indeed, it has been our experience that the sensor performance drifts with time. To quantify this effect we made measurements of the sensor's zero baseline over a period of approximately 60 hours (over a weekend when the laboratory was not occupied), during which time zero air ( $\text{CO}_2$  free) was passed through the test chamber at a low rate (100 cc/min).

The results are shown as a time series in Figure 9, and indicate some large-scale variation in  $S$  that we attribute to temperature changes in the laboratory over the period (the laboratory did not have temperature control).

Using this data, we compiled an Allan deviation plot for  $S$  according to the method set out by Werle *et al* [30] (the Allan deviation  $\sigma$  being the square root of the Allan variance  $\sigma^2$ ). Mean changes in  $\sigma$  as a function of averaging period are shown in Figure 10 and show that for integration periods of a first few minutes, the limit of detection ( $1\sigma$ ) remains around  $3 \times 10^{-5}$  AU. For longer periods, sensor performance is dominated by drift. We believe this is primarily a result of temperature changes (we did not employ temperature compensation during this test) causing changes in detector baseline performance. For example, this can be caused by imperfect matching between the detection and reference elements. The Allan deviation reaches a maximum value of around  $3 \times 10^{-4}$  AU, corresponding to 10 ppm  $\text{CO}_2$ , a factor of 10 worse than the short-term limit of detection.

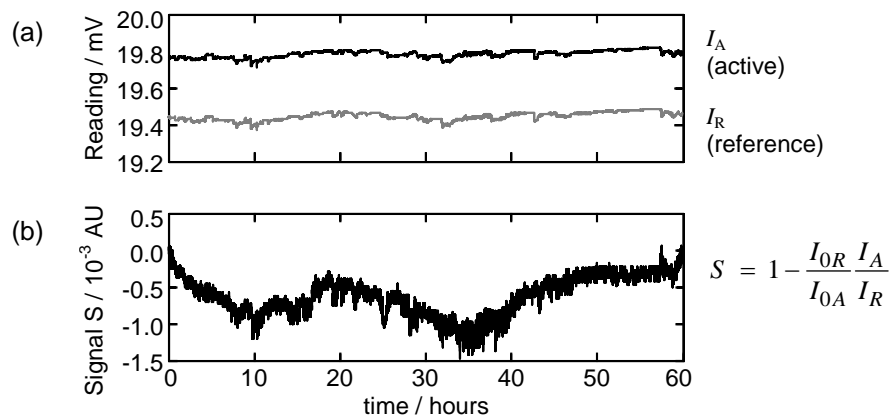


Figure 9. (a) Time series demodulated voltage from active and reference channels responding to zero air over a 60 hour period. (b) Resulting drift in  $S$  (equation (6)) calculated from (a), taking  $I_{0A}$  and  $I_{0R}$  at time  $t = 0$ .

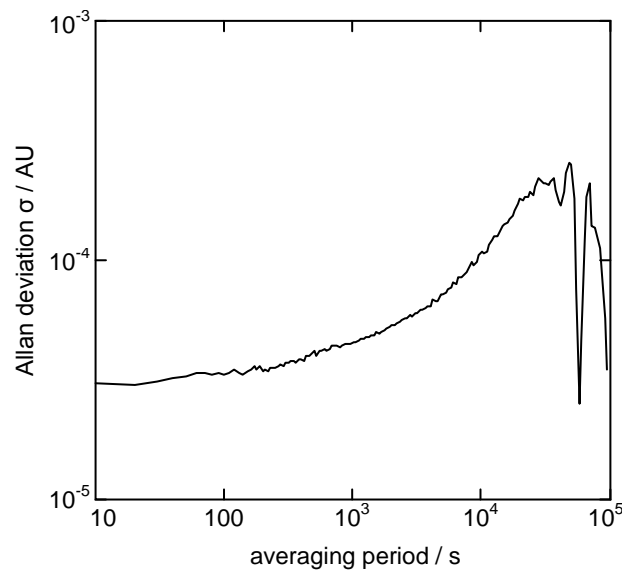


Figure 10. Allan deviation calculated using the data obtained for  $S$  in Figure 9.



### 5.3 Final implementation and field testing

The sensor was also tested using Alphasense proprietary electronics to drive the source and recover signals from the two detectors elements. Here, the drive frequency was 2.25Hz and the source was again modulated with a square wave of peak-to-peak height 5V. Signal recovery in this experiment did not involve the use of a lock-in amplifier, however did use a similar time constant ( $t_{90} = 40s$ ). (Note that the lock-in amplifier used above has a limited choice of time constants, so we were unable to choose exactly comparable values of  $t_{90}$ .) The electronics has been designed to reduce susceptibility to certain drift effects at the source, by delaying signal recovery to the end of each cycle, so as not to be influenced by changes to the warm-up time shown in Figure 7. After the warm-up period, a series of measurements of the signal is made within each modulation cycle. The electronics and subsequent signal processing also provides temperature compensation for the drift effects observed in Figure 9.

We compared the device performance in real-time measurement of  $CO_2$  against an NDIR sensor of identical external dimensions, which is a leading commercially available device. Both the benchmark and our sensor use identical components, namely the microbulb and dual element detector described above. Both devices were left in a laboratory environment and measured ambient air over the course of one day. The results are shown in Figure 11 and show that the two devices gave a similar time series response, and also that our new device showed a lower level of noise.

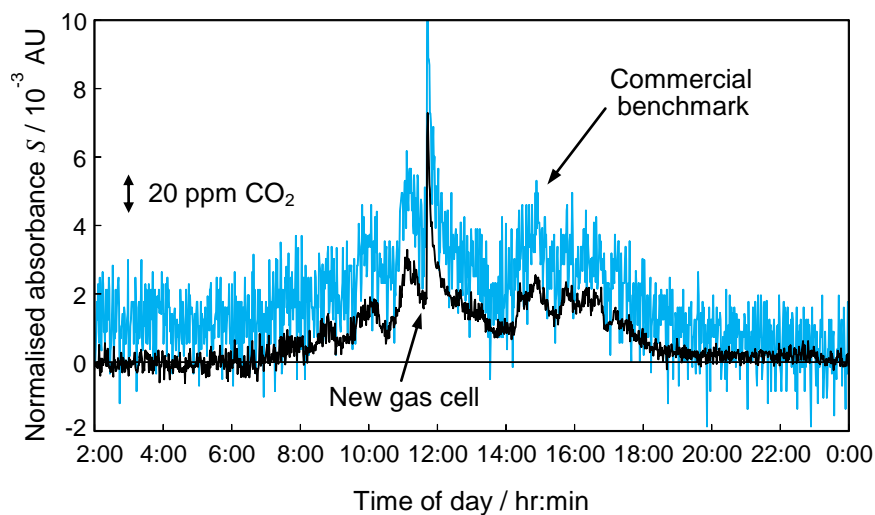


Figure 11. Time series signals  $S$  over the course of one day, measured in the laboratory (deviations from background level). Our device is compared to a benchmark sensor, a leading commercially available  $CO_2$  sensor of the same format. Both sensors were zeroed at 02:00 in ambient air.

## 6 DISCUSSION AND CONCLUSIONS

We have designed, built and evaluated a novel gas sensor design based on the NDIR principle, within the standard miniature format for gas sensors – a cylinder with external dimensions of 20mm diameter x 16.5 mm height. This format is in common use for example in metal oxide semiconductor or electrochemical devices, however such technology is not currently capable of reliably detecting CO<sub>2</sub> at ppm concentrations. Our design pays particular attention to the issue of maintaining a suitable optical pathlength as well as a high optical throughput. To date, there has been little reported analysis of these issues for NDIR devices in the standard miniature format.

Within the sensor are located a dual element detector within a 9mm diameter TO-5 can and an incandescent microbulb light source. It was estimated using raytracing software that 4% of the emitted light reached each of two detector elements with an overall throughput of 0.26 sr mm<sup>2</sup> per detector element. The raytracing software could not account for scattering within the cell and the effect of a join line between the two optical parts; both are expected to reduce efficiency. Nevertheless, we estimated the received RMS modulated light power at 1Hz to have an amplitude of 13 μW after passing through a standard reference bandpass filter (FWHM 0.10 μm, 3.95 μm centre, 80% transmission).

The sensor is most commonly configured for the detection of carbon dioxide, using a dual element detector. The detector integrates matched photodetector elements with bandpass filters, one centred on the CO<sub>2</sub> absorption band at 4.2 μm and the other on a non-absorbing reference band at 3.95 μm. The optical pathlength for the cell has been estimated at 32mm using raytracing software, which is adequate for applications requiring concentration measurements over a wide dynamic range, from low ppm levels to 20% vol. A short-term noise equivalent detection concentration of 1 ppm CO<sub>2</sub> (1σ) has been demonstrated, equivalent to an NEA of 3 x 10<sup>-5</sup> AU. The device has been patented [31] and commercialised as the Alphasense IRC-A1 when configured for measurement of carbon dioxide [32], with a specified zero repeatability over a range of conditions of ±10 ppm CO<sub>2</sub>.

A high optical efficiency offers a number of potential advantages for devices of this type. A high signal to noise ratio enables a low limit of detection, helping to overcome detector noise and baseline drift when using uncooled pyroelectric detectors, which are standard components for this application. Alternatively, two compromises can be made to provide adequate performance in price-sensitive or power-sensitive applications. Firstly, it is possible to use the device with uncooled thermopile detectors, which typically have a higher level of noise than their pyroelectric counterparts [7], yet are less expensive. Secondly, the microbulb may be operated at a lower drive voltage (2V rather than 5V), with a reduced emission intensity but improved lamp output stability, lifetime and power consumption. A high signal to noise ratio may compensate for increased noise levels in these circumstances.

## 7 REFERENCES

- [1] J. Zosel, W. Oelßner, M. Decker, G. Gerlach, U. Guth, The measurement of dissolved and gaseous carbon dioxide concentration, *Meas. Sci. Technol.* 22 (2011), 072001.
- [2] National Building Controls Information Program, Product Testing Report: Wall mounted carbon dioxide (CO<sub>2</sub>) transmitters, NBCIP, Ankeny, IA, USA, 2009.
- [3] G.F. Fine, L.M. Cavanagh, A. Afonja and R. Binions, Metal Oxide Semi-Conductor Gas Sensors in Environmental Monitoring, *Sensors* 10 (2010), 5469-5502.
- [4] S.C. Cutler, A. Vass, Gas Sensor, Patent WO2005054827 (A1), 2005.
- [5] J. Hodgkinson and R. P. Tatam, Optical Gas Sensing: A Review, *Meas. Sci. Technol.* 24 (2013), 012004.
- [6] S.D. Smith, J.G. Crowder, H.R. Hardaway, Recent developments in the applications of mid-infrared lasers, LEDs and other solid state sources to gas detection, *Proc. SPIE* 4651 (2002), 157-172.
- [7] Infratec GmbH, Pyroelectric and multispectral detectors, Product brochure, Infratec GmbH, Dresden, Germany, 2005.
- [8] A.S. Hayward, G.P. Hopkins, Gas sensors, Patent GB 2,395,260, 2005.
- [9] D.M. Stuttard, Gas sensor, Patent WO 02/063283, 2001.
- [10] D.R. Gibson, C. MacGregor, Self powered non-dispersive infra-red CO<sub>2</sub> gas sensor, *J. Phys.: Conf. Ser.* 307 (2011) 012057.
- [11] J. Fonollosa, R. Rubio, S. Hartwig, S. Marco, J. Santander, L. Fonseca, J. Wöllenstein, M. Moreno, Design and fabrication of silicon-based mid infrared multi-lenses for gas sensing applications, *Sensor. Actuat. B* 132 (2008) 498–507.
- [12] J. Fonollosa, B. Halford, L. Fonseca, J. Santander, S. Udina, M. Moreno, J. Hildenbrand, J. Wöllenstein, S. Marco, Ethylene optical spectrometer for apple ripening monitoring in controlled atmosphere store-houses, *Sensor. Actuat. B* 136 (2009) 546–554.
- [13] L. Fonseca, E. Cabruja, C. Calaza, R. Rubio, J. Santander, E. Figueras, I. Gràcia, C. Cané, M. Moreno, S. Marco, Feasibility of a flip-chip approach to integrate an IR filter and an IR detector in a future gas detection cell, *Microsyst. Technol.* 10 (2004) 382-386.
- [14] R. Viola, High-luminosity multipass cell for infrared imaging spectroscopy, *Appl. Opt.* 45 (2006) 2805-2809.
- [15] J. Mayrwöger, P. Hauer, W. Reichl, R. Schwödauier, C. Krutzler, B. Jakoby, Modeling of infrared gas sensors using a ray tracing approach, *IEEE Sens. J.* 10 (2010) 1691-1698.
- [16] J. Mayrwöger, W. Reichl, P. Hauerc, C. Krutzler, B. Jakoby, CO<sub>2</sub> monitoring using a simple Fabry–Perot-based germanium bolometer, *Sensor. Actuat. B* 154 (2011) 245–250.

- [17] I. Sieber, H. Eggert, K.-H. Suphan, O. Nüssen, Optical modelling of the analytical chamber of an IR gas sensor, Proc. SPIE 4408 (2001) 272-282.
- [18] B. Hök, H. Pettersson, A. Kaisdotter Andersson, S. Haasl, P. Åkerlund, Breath analyzer for alcolocks and screening devices, IEEE Sens. J. 10 (2010), 10-15.
- [19] C. Corsi, N. Liberatore, S. Mengali, A. Mercuri, R. Viola, D. Zintu, Advanced applications to Security of IR smart microbolometers, Proc. SPIE 6739 (2007), 673915.
- [20] J.D. Ingle, S.R. Crouch, Spectrochemical Analysis, Prentice Hall, London, 1988.
- [21] Gilway Technical Lamp Inc., Engineering Catalogue 168, Gilway, Woburn, MA, USA, 1999.
- [22] L.S. Rothman, *et al*, The HITRAN 2008 molecular spectroscopic database, J. Quant. Spectrosc. Ra. 110 (2009) 533-572.
- [23] Li-cor Biosciences, LI-7500A open path CO<sub>2</sub>/H<sub>2</sub>O gas analyser, Product specification, Li-cor Biosciences, Lincoln, NA, USA, 2009.
- [24] S.E. Aleksandrov, G.A. Gavrilov, A.A. Kapralov, B.A. Matveev, G.Yu. Sotnikova, M.A. Remennyi, Simulation of characteristics of optical gas sensors based on diode optopairs operating in the mid IR spectral range, Tech. Phys. 54 (2009) 874–881.
- [25] Gilway Technical Lamp, Visible/IR Lamps for NDIR Gas Sensors, Datasheet, Gilway Technical Lamp, Woburn, MA, 1999.
- [26] Zemax EE 2006 version, optical raytrace software package, Zemax, Redmond, WA, USA, 2006.
- [27] W.T. Welford, R. Winston, High collection nonimaging optics, Academic Press, San Diego, USA, 1989.
- [28] J. Hodgkinson, R. Smith, W. O. Ho, J. R. Saffell and R. P. Tatam, A low cost, optically efficient carbon dioxide sensor based on nondispersive infra-red (NDIR) measurement at 4.2µm, Proc SPIE 8349 (2012), 8349-45.
- [29] Mathcad version 14, mathematical analysis software package, PTC Inc, Needham, MA, USA, 2007.
- [30] P. Werle, R. Mücke, F. Slemr, The limits of signal averaging in atmospheric trace-gas monitoring by tunable diode-laser absorption spectroscopy (TDLAS), Appl. Phys. B 57 (1993), 131–139.
- [31] J. Hodgkinson, J.R. Saffell R. Smith, Optical absorption gas sensor, European Patent EP1972923 (A2), 2008.
- [32] Technical specification: IRC-A1 Carbon Dioxide Infrared Sensor, Doc. Ref. IRCA1/JUL12 Alphasense Ltd, Great Notley, Essex, UK, 2012.

## 8 BIOGRAPHIES

Dr Jane Hodgkinson received a BA in Natural Sciences from the University of Cambridge in 1989 and a PhD from the Optoelectronics Research Centre, University of Southampton in 1998. After a career in the chemical, water and gas industries, she joined Cranfield University as a Senior Research Fellow in 2004, funded by an EPSRC Advanced Research Fellowship (2004-2010). Her research into optical gas sensing encompasses non-dispersive infrared detection, tunable diode laser spectroscopy and UV spectroscopy. She serves on the committee of the Gas Analysis and Sensing Group, a UK technology club.

Richard Smith has worked for over 30 years as a Production Design Engineer. Currently he is the Senior Design Engineer at Alphasense where he designs and leads the production of their gas sensors. He is also responsible for the installation of production layouts and bespoke gas calibration facilities at the company. He has previously been a Production Engineer at Neotronics being involved with printed circuit board and instrument assembly of portable gas monitors for the safety and health markets. He was also an Engineer at Corning Medical involved in the manufacture and testing of flame photometers and blood gas analysers.

Dr Wah On Ho received his BSc in Applied Chemistry from the University of Northumbria and his MSc and PhD in Biosensors from the University of Newcastle in 1994. He has held post-doctoral positions at the University of Newcastle and the University of Potsdam, in developing enzyme, antibody and DNA based biosensor systems based on amperometric or impedance transducers. He then moved to a company to develop an electrochemical blood glucose sensor for the diabetic diagnostics market that was commercially successful. Currently he holds a senior scientist position at Alphasense developing their range of non-dispersive infra-red and ozone gas sensors.

Dr John R Saffell has been Technical Director of Alphasense Ltd since it was founded in 1997. Dr Saffell has a BSc in chemistry from MIT (1975) and PhD in materials science from Cambridge University (1979). He has been involved in gas sensing and water quality measurement for 30 years and is responsible for working with Universities to develop and exploit new gas sensing technologies. He is Chairman of the Council of Gas Detection and Environmental Measurement (CoGDDEM) and previous Chairman of Sensors for Water Interest Group (SWIG).

Professor Ralph P Tatam gained a BSc from the University of Exeter (1981) and a PhD (Physics) from the City of London Polytechnic (1986). He worked in the Physics Laboratory at the University of Kent before joining Cranfield, where he is now Head of the Department of Engineering Photonics and recently completed 3.5 years as Dean of Faculty. He has a DSc from the University of Exeter, is a Fellow of the SPIE, and was elected to its Board of Directors (2010-2012). His research aims to develop novel optical instrumentation to better understand physical phenomena, and encompasses optical fibre sensors, speckle interferometry, laser Doppler anemometry, optical coherence tomography and gas sensing. He has published >400 papers.